Structural basis for the inhibition of COVID-19 virus main protease by carmofur, an antineoplastic drug

Author

Zhenming Jin[1,2*], Yao Zhao[1*], Yuan Sun[3*], Bing Zhang[1], Haofeng Wang[1,4], Yan Wu[3], Yan Zhu[1], Chen Zhu[1], Tianyu Hu[1], Xiaoyu Du[1,2], Yinkai Duan[1], Jing Yu[1], Xiaobao Yang[1], Xiuna Yang[1], Xiang Liu[5], Luke W. Guddat[6], Gengfu Xiao[3], Leike Zhang[3†], Haitao Yang[1†] & Zihe Rao[1,2,5]

[1]Shanghai Institute for Advanced Immunochemical Studies and School of Life Science and Technology, ShanghaiTech University, Shanghai, China.

[2]Laboratory of Structural Biology, School of Life Sciences and School of Medicine, Tsinghua University, Beijing, China.

[3]State Key Laboratory of Virology, Wuhan Institute of Virology, Center for Biosafety Mega-Science, Chinese Academy of Sciences, Wuhan, China.

[4]School of Life Sciences, Tianjin University, Tianjin, China

[5]State Key Laboratory of Medicinal Chemical Biology, Frontiers Science Center for Cell Response, College of Life Sciences, College of Pharmacy, Nankai University, Tianjin, China.

[6]School of Chemistry and Molecular Biosciences, the University of Queensland, Brisbane, Australia.

[*]These authors contributed equally: Zhenming Jin, Yao Zhao and Yuan Sun.

[†]e-mail: zhangleike@wh.iov.cn; yanght@shanghaitech.edu.cn

Abstract

COVID-19 virus is the cause of a debilitating and life-threatening infectious pulmonary disease that is now responsible for a global pandemic. Currently, there are no specific drugs or vaccines to contain this virus. The main protease (M^{pro}) of COVID-19 virus is a key enzyme, which plays an essential role in viral replication and transcription, making it an ideal drug target. An FDA-approved antineoplastic drug, carmofur, has been identified as an inhibitor that targets COVID-19 virus M^{pro}. However, its inhibitory mechanism is unknown. Here, we report the 1.6-Å crystal structure of COVID-19 virus M^{pro} in complex with carmofur. The crystal structure shows that carmofur contains an electrophilic carbonyl reactive group, which covalently binds to C145, a member of the catalytic dyad. As a result, its fatty acid tail occupies the hydrophobic S2 subsite of M^{pro} whilst its 5-fluorouracil head is cleaved as product of the new covalent bond that has formed. Carmofur is active in a cell based antiviral assay with an EC_{50} of 24.87 μM. It is therefore a promising lead compound for the development of new antivirals to target COVID-19.

Introduction

Starting in December 2019, a highly infectious viral disease has now spread and reached over 200 countries leading to a global public health emergency and pandemic. The etiological agent of the disease is a coronavirus (identified as COVID-19). According to the WHO COVID-2019 Situation Report-77, there were 1,210,956 confirmed cases and 67,594 deaths, with a mortality rate at 5.58%. The number of confirmed cases worldwide continues to grow at a rapid rate and is far from peaking. However, there are no specific drugs or vaccines available to control symptoms or the spread of this disease.

The COVID-19 virus has a ~30,000 nt RNA genome encoded with two translation products, polyproteins 1a and 1ab (pp1a and pp1ab) which are crucial for replication and transcription[1,2]. These polyproteins become matured non-structural and structural proteins through auto-cleavage by the main protease (M^{pro}) and by a papain-like protease[3]. Because of this, M^{pro} is an excellent target for anti-coronavirus (CoV) drug development[4-6]. In order to rapidly discover new drug leads that target COVID-19 virus M^{pro}, our group screened over 10,000 compounds from a library that consisted of approved drugs, drug candidates in clinical trials, and other pharmacologically active compounds. Amongst these we identified carmofur as compound that can inhibit M^{pro} with an IC_{50} of 1.82 μM [7].

Carmofur is an FDA-approved antineoplastic drug, and a derivative of 5-fluorouracil (5-FU) a widely drug used against solid cancers. 5-FU is especially efficient for controlling head, neck, and gastrointestinal tumors[8]. Carmofur (Figure 1A) is a derivative of this compound and has been used in colon cancer therapy since 1981[9]. Clinical research has also shown that carmofur has a curative effect on breast, gastric, bladder, and colorectal cancers[10-12]. The target for carmofur is believed to be thymidylate synthase an enzyme that converts deoxy uridine monophosphate (dUMP) to deoxythymidine monophosphate[13,14]. Carmofur has also been shown to target human acid ceramidase (AC)[15], a potential drug target for the treatment of melanoma and glioblastoma tumors[16,17]. Carmofur inhibits human AC through the covalent modification of its catalytic cysteine[18]. Our previous data shows that carmofur inhibits M^{pro} activity[7], but the molecular details as to how it inhibits this target are unresolved. Here, we have determined the 1.6-Å crystal structure of COVID-19 virus M^{pro} in complex with this compound. The structure shows that the fatty acid tail from carmofur

covalently binds to C145 at the catalytic center of the viral protease (Figure 1B). Furthermore, cell-based assays show that carmofur has an EC_{50} value of ~25 μM for the COVID-19 virus. This high-resolution crystal structure thus provides the structural basis for the design of new carmofur analogs with clinical potential to treat COVID-2019.

Results

Overall structure of M^{pro}-carmofur complex

The structure of COVID-19 virus M^{pro} in complex with the fatty acid tail of carmofur has been solved at a resolution of 1.6 Å (Extended Data Table 1). In accord with our previous studies[4,5,19-21], this M^{pro} complex also forms a homodimer. In the crystal structure, this is formed by two polypeptides (protomer A and B) related by crystallographic symmetry (Figure 1C). All of the residues, 1–306, in the polypeptide could be traced in the electron density map. Each protomer is composed of three domains, similar to those found in other M^{pro} structures (Figure 1A). Domain I (residues 10–99) and domain II (residues 100–184) are two β-sheet rich domains. Domain III (residues 201–303) is linked to domain II by a long loop region (residues 185–200). The buried surface area at the dimer interface is ~1409 $Å^2$. This is mainly due to interactions by domain II, domain III and the N-termini of each polypeptide.

There are twelve cysteine residues across the protein with six buried in the core (Figure S3). The other six cysteines are exposed to the surface, with one of these (C145) located in the catalytic center, which lies in a cleft between domain I and domain II. The long loop connecting domain II and domain III also participates in the formation of the substrate binding pocket. S1 of one protomer interacts with E166 of the neighbor protomer to stabilize the S1 subsite of the substrate-binding pocket. This structural feature is essential for catalysis.

Carmofur is covalently linked to the catalytic cysteine

The substrate-binding pocket lies in the cleft between domain I and domain II and is characterized by the presence of the catalytic dyad residues, C145 and H41 (Figure 2A, 2B). The electron density map unambiguously shows that the fatty acid moiety ($C_7H_{14}NO$) of carmofur is linked to the Sγ atom of C145 through a 1.8-Å covalent bond, and that the fatty acid tail is inserted into the S2 subsite (Figure 2B, 2C). It suggests

that the sulfhydryl group of catalytic C145 attacks the electrophilic carbonyl group of carmofur, resulting in the covalent modification of the cysteine residue by the fatty acid moiety ($C_7H_{14}NO$) and the release of the 5-fluorouracil head (Figure S1A). This result is also consistent with our previous tandem MS/MS studies[7].

In addition to the C-S covalent bond, the inhibitor is stabilized by numerous hydrogen bonds and hydrophobic interactions (Figure 2C, S1B). The carbonyl oxygen of the inhibitor occupies the oxyanion hole and forms hydrogen bonds (3.0-Å) with the backbone amides of C143 and C145, mimicking the tetrahedral oxyanion intermediate formed during protease cleavage (Figure 2C). The fatty acid tail, which presents in an extended conformation, inserts into the bulky hydrophobic S2 subsite (composed of the side chains of H41, M49, Y54, M165, and the alkyl portion of the side chain of D187) (Figure 2B, 2C). The hydrophobic interactions are mainly contributed by the side chains of H41, M49 and M165, all of which run parallel with the alkyl part of the fatty acid tail of the inhibitor (Figure 2C, S1B).

Compared with that for the Michael acceptor, inhibitor N3[7,22], the covalent modification mechanism for carmofur is different. In this case, the catalytic C145 attacks the electrophilic carbonyl group of carmofur and results in the covalent modification of the cysteine residue while in the case of N3, covalent modification occurred through Michael addition of the vinyl group.

The overall structures of the M^{pro}-carmofur complex and the M^{pro}N3 complex are similar with an RMSD of 0.286 Å for all Cα atoms. Though slight, the largest conformational differences occur in the substrate binding pocket (Figure S2A). Compared with the M^{pro}-N3 complex structure, the backbone surrounding the inhibitor binding site of carmofur complex structure moves in a slightly outward direction (Figure S2A). A major difference between N3 and carmofur binding is that N3 occupies four subsites (S1, S2, S4 and S1′), (Figure S2B) whereas carmofur only occupies the S2 subsite. Thus, there is good scope for structural elaboration of this lead. Interestingly, a molecule of DMSO fills the S1 subsite, a region corresponding to the location where the lactam ring in the N3 bound complex is located (Figure S2B). This observation should also assist in the design of more potent carmofur analogs as inhibitors of COVID-19 M^{pro}.

Antiviral activity assay

In our preliminary antiviral studies reported recently[7], at a concentration of 10 μM treatment in COVID-19 virus infected Vero cells, ebselen showed potent antiviral effect while carmofur did not demonstrate strong antiviral activity at this concentration. It indicates that carmofur have a larger EC_{50} value than that for Ebselen (EC_{50}=4.67 μM). We then set out to determine the accurate EC_{50} value for carmofur. As described in our previous study[23], Vero E6 cells were treated with a series of concentrations of carmofur, and were then were infected with COVID-19 virus. As a result, the EC_{50} for carmofur was determined to be 24.87 μM (Figure 3B). To verify this result, infected cells were fixed and subjected to immunofluorescence assay (IFA) using anti-sera against viral nucleocapsid protein (NP). Figure 3A shows NP expression levels decreased after the treatment of carmofur, in accordance with the quantitative RT-PCR study. A cytotoxicity assay was also performed in Vero E6 cells with a CC_{50} value of 132.7 μM (Figure 3C). Thus, the compound has a favorable selectivity index (SI) of 5.34, but optimization is needed to make it an effective drug.

Discussion

In conclusion, we have solved the 1.6-Å crystal structure of M^{pro} in complex with an FDA approved antineoplastic, carmofur. This study shows that carmofur directly modifies the catalytic cysteine of COVID-19 virus M^{pro} leading to its inhibition. The study also provides a basis for rational design of carmofur analogs to treat COVID-19 infections. Since M^{pro} is highly conserved among all CoV M^{pro}s, carmofur and carmofur analogs could also be effective against other CoV M^{pro}s.

We also showed that carmofur can inhibitor COVID-19 virus at a lower concentration than its cellular cytotoxicity (SI > 5), further suggesting that carmofur is a good starting point to develop inhibitors with clinical potential to treat COVID-19. In addition, it has been reported that carmofur might be a novel therapeutic agent for acute lung injury (ALI)[24] which can also benefit COVID-19 patients since lung injury is an outcome that can occur as the result of this infection.

References

1. Wu, F. et al. A new coronavirus associated with human respiratory disease in China. *Nature* **579**, 265-269 (2020).
2. Zhou, P. et al. A pneumonia outbreak associated with a new coronavirus of probable bat origin. *Nature* **579**, 270-273 (2020).
3. Hegyi, A. & Ziebuhr, J. Conservation of substrate specificities among coronavirus main proteases. *J Gen Virol* **83**, 595-599 (2002).
4. Anand, K. et al. Structure of coronavirus main proteinase reveals combination of a chymotrypsin fold with an extra alpha-helical domain. *Embo j* **21**, 3213-24 (2002).
5. Yang, H. et al. The crystal structures of severe acute respiratory syndrome virus main protease and its complex with an inhibitor. *Proc Natl Acad Sci U S A* **100**, 13190-5 (2003).
6. Pillaiyar, T., Manickam, M., Namasivayam, V., Hayashi, Y. & Jung, S.H. An Overview of Severe Acute Respiratory Syndrome-Coronavirus (SARS-CoV) 3CL Protease Inhibitors: Peptidomimetics and Small Molecule Chemotherapy. *J Med Chem* **59**, 6595-628 (2016).
7. Jin, Z. et al. Structure of Mpro from COVID-19 virus and discovery of its inhibitors. *bioRxiv*, 2020.02.26.964882 (2020).
8. Sara, J.D. et al. 5-fluorouracil and cardiotoxicity: a review. *Ther Adv Med Oncol* **10**, 1758835918780140 (2018).
9. Sakamoto, J. et al. An individual patient data meta-analysis of adjuvant therapy with carmofur in patients with curatively resected colon cancer. *Jpn J Clin Oncol* **35**, 536-44 (2005).
10. Liu, P., Ma, S., Liu, H., Han, H. & Wang, S. HCFU inhibits cervical cancer cells growth and metastasis by inactivating Wnt/β-catenin pathway. *J Cell Biochem* (2017).
11. Gröhn, P. et al. Oral carmofur in advanced gastrointestinal cancer. *Am J Clin Oncol* **13**, 477-9 (1990).
12. Maehara, Y., Anai, H., Kusumoto, H., Kusumoto, T. & Sugimachi, K. Colorectal carcinoma in vitro is more sensitive to 1-hexylcarbamoyl-5-fluorouracil compared with six other antitumor drugs: carboquone, Adriamycin, mitomycin C, aclacinomycin A, cisplatin, 5-fluorouracil. *Dis Colon Rectum* **31**, 62-7 (1988).
13. Ooi, A. et al. Plasma, intestine and tumor levels of 5-fluorouracil in mice bearing L1210 ascites tumor following oral administration of 5-fluorouracil, UFT (mixed compound of tegafur and uracil), carmofur and 5'-deoxy-5-fluorouridine. *Biol Pharm Bull* **24**, 1329-31 (2001).
14. Sato, S., Ueyama, T., Fukui, H., Miyazaki, K. & Kuwano, M. [Anti-tumor effects of carmofur on human 5-FU resistant cells]. *Gan To Kagaku Ryoho* **26**, 1613-6 (1999).
15. Nguyen, H.S., Awad, A.J., Shabani, S. & Doan, N. Molecular Targeting of Acid Ceramidase in Glioblastoma: A Review of Its Role, Potential Treatment, and Challenges. *Pharmaceutics* **10**(2018).
16. Lai, M. et al. Complete Acid Ceramidase ablation prevents cancer-initiating cell formation in melanoma cells. *Sci Rep* **7**, 7411 (2017).
17. Doan, N.B. et al. Acid ceramidase and its inhibitors: a de novo drug target and a new class of drugs for killing glioblastoma cancer stem cells with high efficiency. *Oncotarget* **8**, 112662-112674 (2017).
18. Dementiev, A. et al. Molecular Mechanism of Inhibition of Acid Ceramidase by Carmofur. *J Med Chem* **62**, 987-992 (2019).
19. Xue, X. et al. Structures of two coronavirus main proteases: implications for substrate binding and antiviral drug design. *J Virol* **82**, 2515-27 (2008).
20. Ren, Z. et al. The newly emerged SARS-like coronavirus HCoV-EMC also has an "Achilles' heel": current effective inhibitor targeting a 3C-like protease. *Protein Cell* **4**, 248-50 (2013).
21. Wang, F., Chen, C., Tan, W., Yang, K. & Yang, H. Structure of Main Protease from Human Coronavirus NL63: Insights for Wide Spectrum Anti-Coronavirus Drug Design. *Sci Rep* **6**, 22677 (2016).
22. Yang, H. et al. Design of wide-spectrum inhibitors targeting coronavirus main proteases. *PLoS Biol* **3**, e324 (2005).
23. Wang, M. et al. Remdesivir and chloroquine effectively inhibit the recently emerged novel coronavirus (2019-nCoV) in vitro. *Cell Res* **30**, 269-271 (2020).
24. Wu, K., Xiu, Y., Zhou, P., Qiu, Y. & Li, Y. A New Use for an Old Drug: Carmofur Attenuates Lipopolysaccharide (LPS)-Induced Acute Lung Injury via Inhibition of FAAH and NAAA Activities. *Front Pharmacol* **10**, 818 (2019).
25. Kabsch, W. *XDS*. *Acta Crystallogr D Biol Crystallogr* **66**, 125-132 (2010).

26. McCoy, A.J. et al. Phaser crystallographic software. *J Appl Crystallogr* **40**, 658-674 (2007).
27. Liebschner, D. et al. Macromolecular structure determination using X-rays, neutrons and electrons: recent developments in Phenix. *Acta Crystallogr D Struct Biol* **75**, 861-877 (2019).
28. Emsley, P., Lohkamp, B., Scott, W.G. & Cowtan, K. Features and development of Coot. *Acta Crystallogr D Biol Crystallogr* **66**, 486-501 (2010).
29. Afonine, P.V. et al. Towards automated crystallographic structure refinement with phenix.refine. *Acta Crystallogr D Biol Crystallogr* **68**, 352-67 (2012).

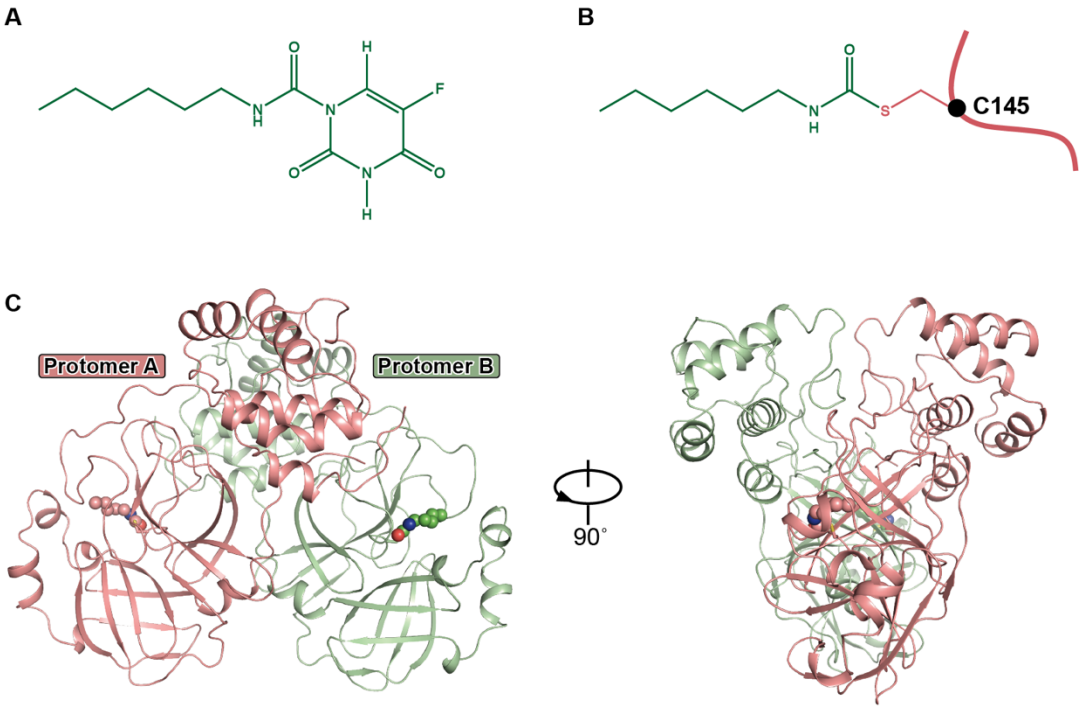

Figure 1. Overall structure of COVID-19 virus M^{pro} in complex with carmofur

A. The chemical structure of carmofur.

B. The binding mode of carmofur to COVID-19 virus M^{pro}. The red curve represents COVID-19 virus M^{pro} polypeptide with the sidechain of Cys145 protruding.

C. The overall structure of COVID-19 virus M^{pro} in complex with carmofur. The salmon and green represent the different protomers. The carmofur atoms are shown as solid spheres.

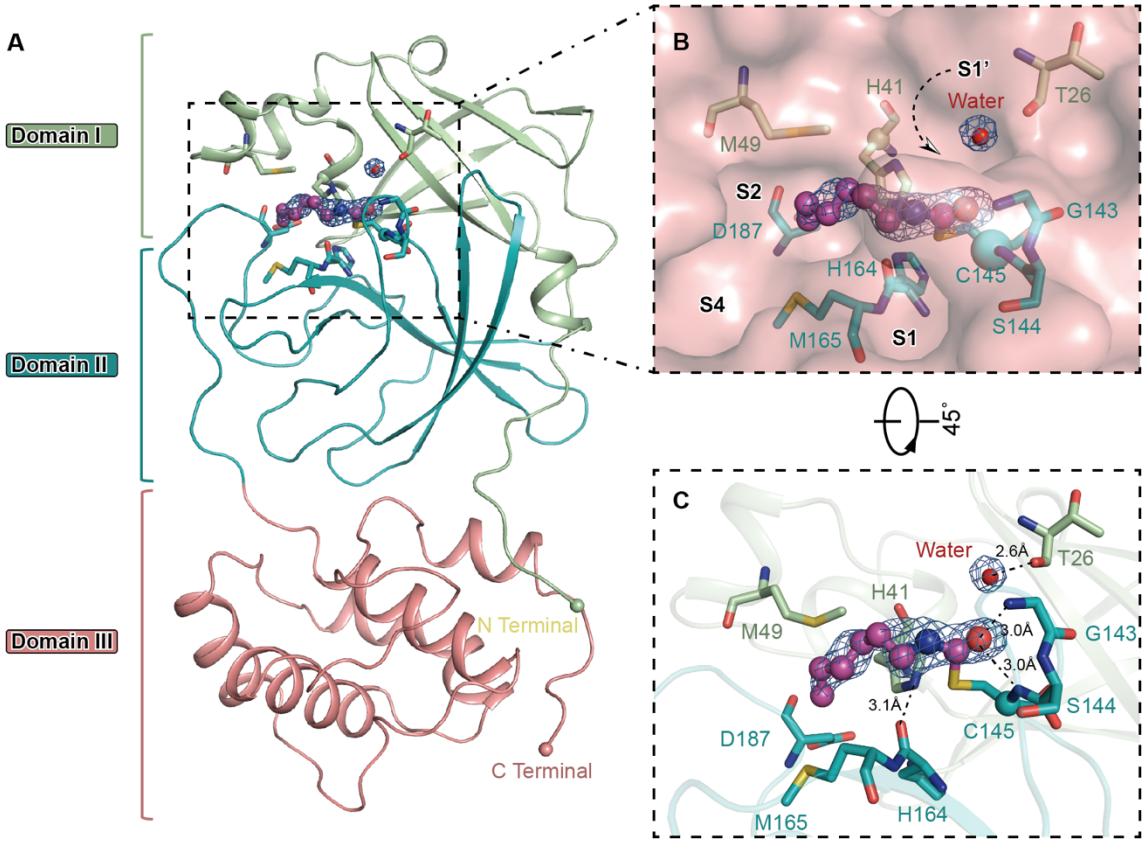

Figure 2. Catalytic center of the COVID-19 virus M^{pro}-carmofur complex

A. The structure of a single protomer. The three domains are shown in three different colors. The catalytic center is located within the dashed square.

B. Zoom in of the catalytic center. The residues that participate in carmofur binding are shown as stick models. Carmofur is show as a ball and stick model with the carbons in magenta. Water is presented as a red sphere.

C. A rotated view of the binding site, but with the surface removed.

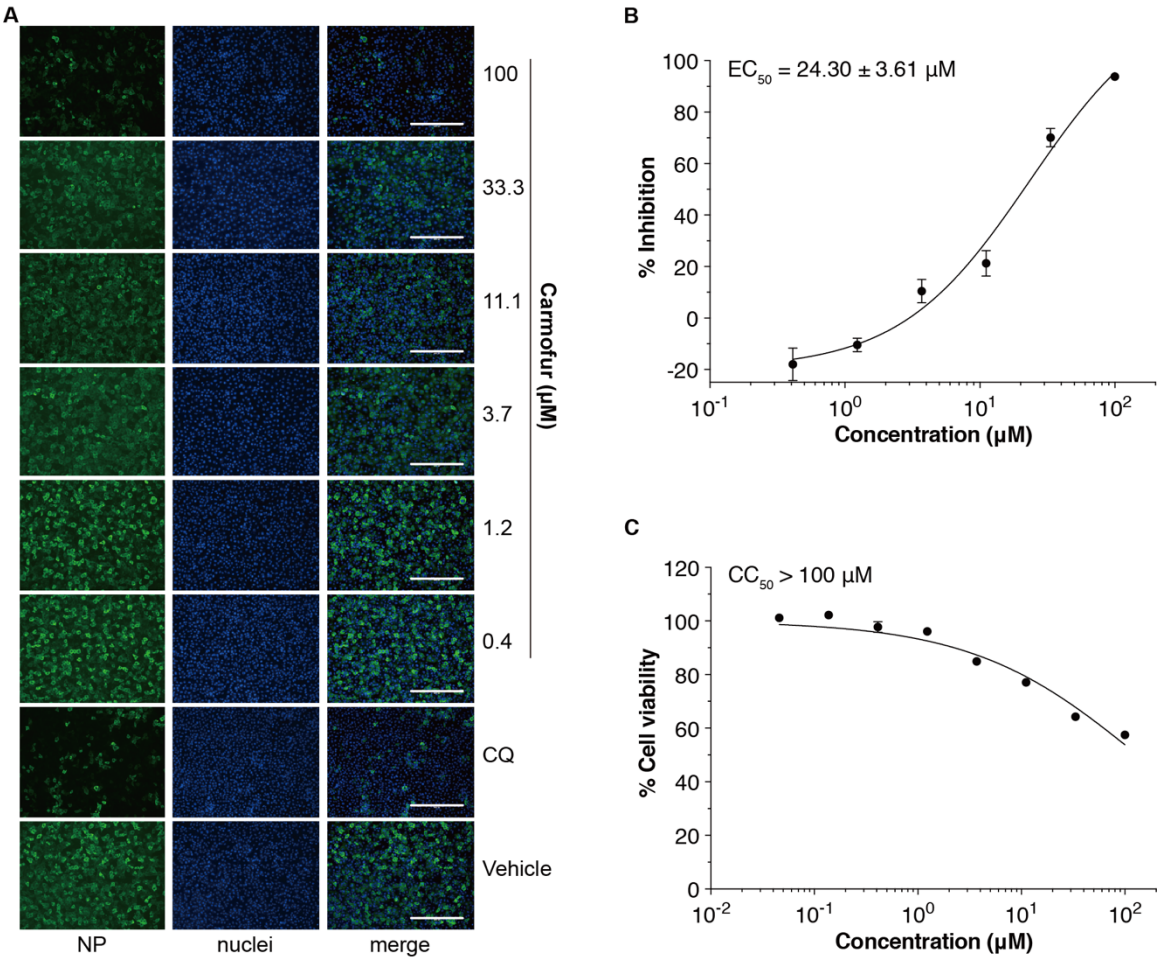

Figure 3. Inhibition of SARS-CoV-2 by carmofur in Vero E6 cells

Vero E6 cells infected with SARS-CoV-2 at a MOI of 0.05 were treated with carmofur at a range of different concentrations.

A. At 24 hours p.i., cells were fixed, and intracellular NP levels were monitored by immunofluorescence. Chloroquine (CQ, 10 μM) was used as a positive control. Bars: 400 μm

B. Cell viability was measured using a CCK8 assay. The Y-axis represents mean % of cell viability. The experiments were performed in triplicate, and data shown are for the mean values ± SE.

C. Supernatant was collected and viral copy number in the supernatant was measured with quantitative RT-PCR. The Y-axis of the graph indicates mean % inhibition of virus, the experiments were performed in triplicate, and data shown are mean values ± SE.

Methods

Cloning, protein expression and purification of COVID-19 virus M^{pro}

The cell cultures were grown and the protein expressed according to a previous report[7]. The cell pellets were resuspended in lysis buffer (20mM Tris-HCl pH 8.0, 150 mM NaCl, 5% Glycerol), lysed by high-pressure homogenization, and then centrifuged at 25,000g for 30 min. The supernatant was loaded onto Ni-NTA affinity column (Qiagen, Germany), and washed by the lysis buffer containing 20 mM imidazole. The His tagged M^{pro} was eluted by lysis buffer that included 300 mM imidazole. The imidazole was then removed through desalting. Human rhinovirus 3C protease was added to remove the C-terminal His tag. COVID-19 virus M^{pro} was further purified by ion exchange chromatography. The purified M^{pro} was transferred to 10 mM Tris-HCl pH 8.0 through desalting and stored at -80 degrees until needed.

Crystallization, data collection and structure determination

COVID-19 virus M^{pro} was concentrated to 5 mg/ml incubated with 0.3 mM carmofur for 1 hour and the complex was crystallized by hanging drop vapor diffusion method at 20 °C. The best crystals were grown using a well buffer containing 0.1 M MES pH 6.0, 5% polyethylene glycol (PEG) 6000, and 3% DMSO. The cryo-protectant solution was the reservoir but with 20% glycerol added.

X-ray data were collected on beamline BL17U1 at Shanghai Synchrotron Radiation Facility (SSRF) at 100 K and at a wavelength of 0.97918 Å using an Eiger X 16M image plate detector. Data integration and scaling were performed using the program XDS[25]. The structure was determined by molecular replacement (MR) with the PHASER[26] and Phenix 1.17.1 [27] using the COVID-19 virus M^{pro} (PDB ID: 6LU7) as a search template. The model from MR was subsequently subjected to iterative cycles of manual model adjustment with Coot 0.8 [28] and refinement was completed with Phenix REFINE[29]. The inhibitor, carmofur, was built according to the omit map. The phasing and refinement statistics are summarized in Extended Data Table 1. Coordinates and structure factors have been deposited in Protein Data Bank (PDB) with accession number 7BUY.

Antiviral and cytotoxicity assays for carmofur

A clinical isolate COVID-19 virus (nCoV-2019BetaCoV/Wuhan/WIV04/2019) was propagated in Vero E6 cells, and viral titer was determined as described previously[23]. For the antiviral assay, pre-seeded Vero E6 cells (5×10^4 cells/well) were pre-treated with the different concentration of carmofur for 1 h and the virus was subsequently added (MOI of 0.05) to allow infection for 1 h. Next, the virus-drug mixture was removed, and cells were further cultured with fresh drug containing medium. At 24 h p.i. (post infection), the cell supernatant was collected and vRNA in supernatant was subjected to qRT-PCR analysis, while cells were fixed and subjected to immunofluorescence to monitor intracellular NP level as described previously[23]. For cytotoxicity assays, Vero E6 cells were suspended in growth medium in 96-well plates. The next day, appropriate concentrations of carmofur were added to the medium. After 24 h, the relative numbers of surviving cells were measured by the CCK8 (Beyotime, China) assay in accordance with the manufacturer's instructions. All experiments were performed in triplicate, and all the infection experiments were performed at biosafety level-3 (BSL-3).

Acknowledgement

We are grateful to the staff at the BL17U beamline of the Shanghai Synchrotron Radiation Facility (SSRF), where data were collected. This work was supported by grants from National Key R&D Program of China (grant No. 2017YFC0840300 to Z.R.), National Key R&D Program of China (grant No. 2020YFA0707500 to Z.R.), Project of International Cooperation and Exchanges NSFC (grant No. 81520108019 to Z.R.), Science and Technology Commission of Shanghai Municipality (grant No. 20431900200), Department of Science and Technology of Guangxi Zhuang Autonomous Region (grant No. 560 2020AB40007), and the Natural Science Foundation of China (grant No. 31970165 to Leike Zhang.

Author contributions

Z.R. and H.Y. conceived the project; Z.J., Y.Z., Z.R., and H.Y. designed the experiments; Y.Z., Z.J., H.W., Y. Zhu., C.Z., X.D. J.Y. and X.Y. cloned, expressed, purified and crystallized proteins; Y.Z., B.Z., Z.J. and T.H. collected the diffraction data; Y.Z, B.Z. and Xiang Liu solved the crystal structure; Y.S., and Y.W. performed cell-based antiviral assay; Y.D. and L. Z performed qRT-PCR and cytotoxicity assay

332 analysis; Y.Z., J.Z., L.Z., Y.D., X. L., L.G., G.X., Z.R. and H.Y. analyzed and discussed
333 the data; Y.Z., Z.J., L.Z., L.G. H.Y, and Z.R. wrote the manuscript.

334 **Competing interests**

335 The authors declare no competing interests.

336

337 **Data and materials availability**

338 The PDB accession No. for the coordinates of COVID-19 virus M^{pro} in complex with
339 carmofur is 7BUY.

340

341 **Table S1. Data collection and refinement statistics**
342

Data collection	
Space group	*C*2
Wavelength (Å)	0.979
Cell dimensions	
a, b, c (Å)	98.03, 81.65, 51.64
α, β, γ (°)	90, 114.879, 90
Resolution (Å)	46.85-1.60 (1.64-1.60) [a]
Completeness (%)	99.2 (98.9)
R_{merge} (%)	3.4 (50.9)
$CC_{1/2}$	99.8 (85.9)
Redundancy	3.4 (3.4)
Mean $I/\sigma(I)$	17.25 (2.37)
Refinement	
Resolution (Å)	25.64-1.6 (1.66-1.60)
No. of reflections	48563 (4843)
R_{work}/R_{free} (%)	18.59 (27.98)/20.34 (32.43)
No. of non-hydrogen atoms	2601
Protein	2367
Ligands	29
Solvent	205
Average *B*-factor (Å^2)	38.74
Protein	37.91
Ligands	52.55
Solvent	46.40
R.m.s deviations	
Bond lengths (Å)	0.016
Bond angles (°)	1.370
Ramachandran plot (%)	
Favored	97.37
Allowed	2.63
Outliers	0.00

343 [a] Values in parentheses are for highest-resolution shell.
344

345

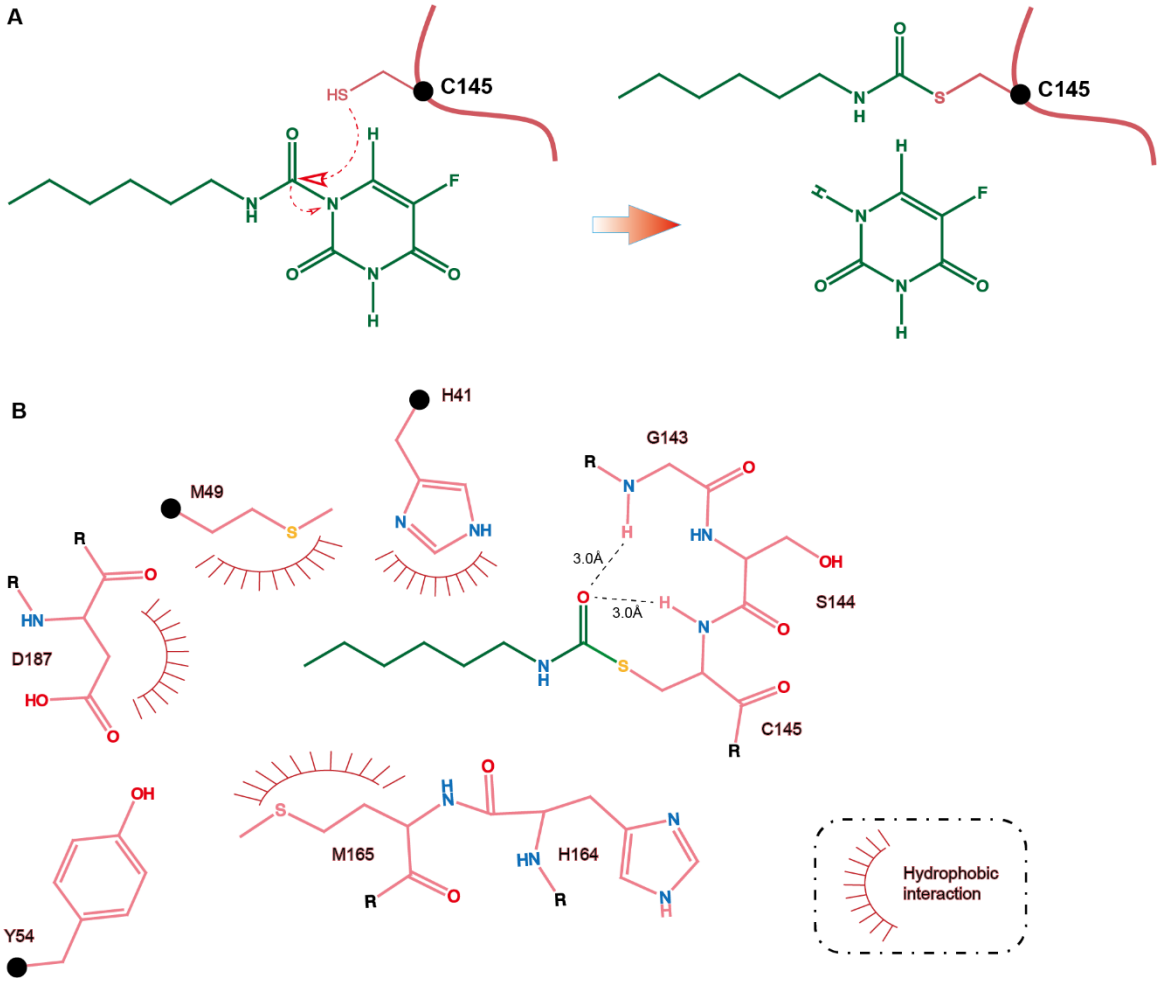

Figure S1. Inhibition of M^{pro} by carmofur

A. Putative inhibition mechanism. Red curve represents M^{pro} polypeptide and the black sphere represent the Cα of C145.

B. Schematic diagram of M^{pro}-carmofur interactions. Black spheres represent Cα atoms.

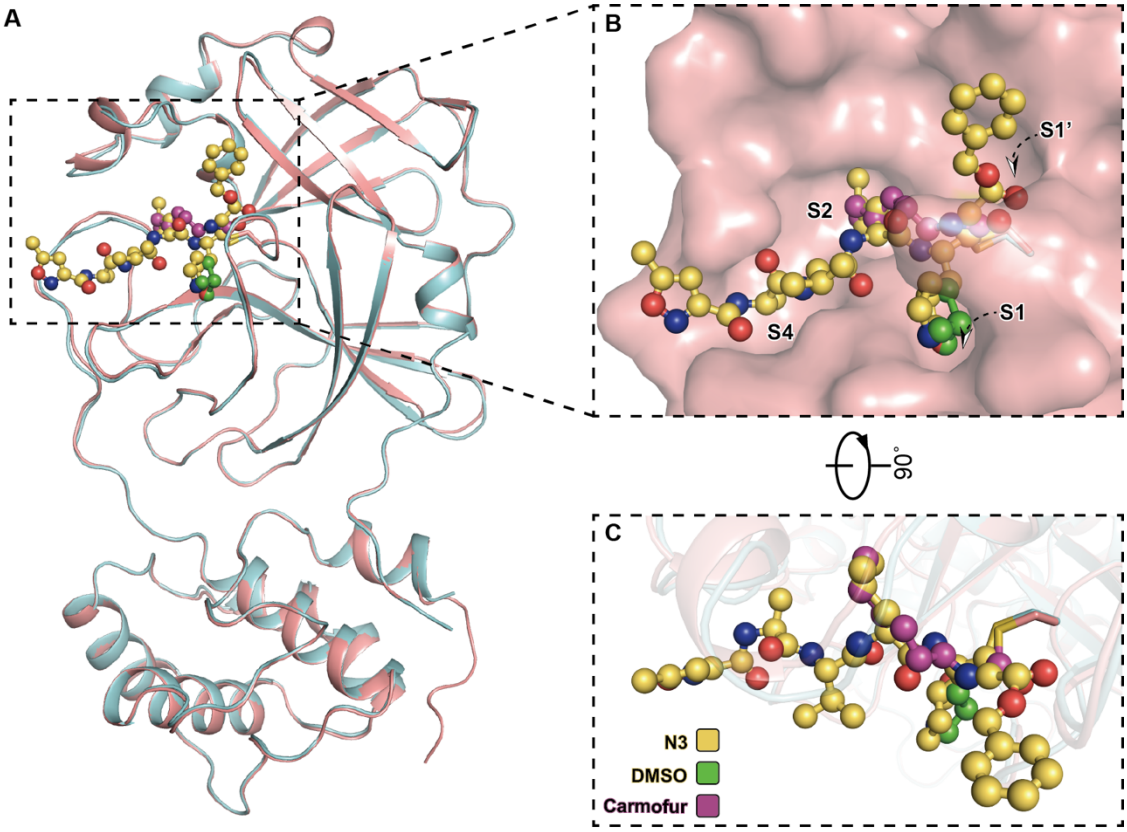

Figure S2. Binding mode of carmofur and N3 to M^{pro}.

A. Overall structural comparison between the M^{pro}-carmofur and M^{pro}-N3 complexes. The salmon cartoon represents the carmofur bound structure and the light cyan represents the N3 bound structure. Carmofur, N3 and DMSO are represented by the purple, yellow and green balls and sticks, respectively.

B. The binding pocket of M^{pro}. Carmofur and N3 are represent in the same way as in Figure S2A.

C. Schematic diagram of carmofur and N3.

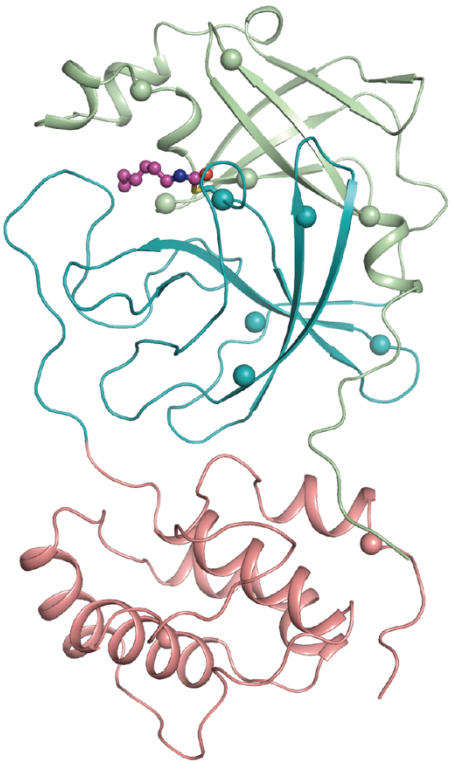

Figure S3. Cysteine residues in M^{pro}

Each cysteine side chain is represented by a colored sphere.